BBA - Bioenergetics 1860 (2019) 508–518

Contents lists available at ScienceDirect

BBA - Bioenergetics

journal homepage: www.elsevier.com/locate/bbabio

Temperature dependence of the high-spin S_2 to S_3 transition in Photosystem II: Mechanistic consequences

Alain Boussac

I2BC, CNRS UMR 9198, CEA Saclay, 91191 Gif sur Yvette, France

ARTICLE INFO

Keywords:
Photosystem II
Oxygen evolution
Mn_4CaO_5 cluster
Spin state
EPR

ABSTRACT

The Mn_4CaO_5-cluster in Photosystem II advances through five oxidation states, S_0 to S_4, before water is oxidized and O_2 is generated. The S_2-state exhibits either a low-spin, $S = 1/2$ (S_2^{LS}), or a high-spin state, $S = 5/2$ (S_2^{HS}). Increasing the pH favors the S_2^{HS} configuration and mimics the formation of $Tyr_Z^{\cdot}$ in the S_2^{LS}-state at lower pH values (Boussac et al. Biochim. Biophys. Acta 1859 (2018) 342). Here, the temperature dependence of the S_2^{HS} to S_3 transition was studied by EPR spectroscopy at pH 8.6. The present data strengthened the involvement of S_2^{HS} as a transient state in the $S_2^{LS}Tyr_Z^{\cdot} \rightarrow S_2^{HS}Tyr_Z^{\cdot} \rightarrow S_3Tyr_Z$ transition. Depending on the temperature, the S_2^{HS} progresses to S_3 states exhibiting different EPR properties. One S_3-state with a $S = 3$ signal, supposed to have a structure with the water molecule normally inserted in S_2 to S_3 transition, can be formed at temperatures as low as 77 K. This suggests that this water molecule is already bound in the S_2^{HS} state at pH 8.6. The nature of the EPR invisible S_3 state, formed down to 4.2 K from a S_2^{HS} state, and that of the EPR detectable S_3 state formed down to 77 K are discussed. It is proposed that in the S_2^{LS} to S_3 transition, at pH $<$ 8.6, the proton release (Sugiura et al. Biochim. Biophys. Acta 1859 (2018) 1259), the S_2^{LS} to S_2^{HS} conversion and the binding of the water molecule are all triggered by the formation of $Tyr_Z^{\cdot}$.

1. Introduction

The input of energy into the living world is provided by the oxygenic photosynthesis. Photosynthesis produces fibers, foods and fossil fuels. Photosystem II (PSII), the water-oxidizing enzyme of the cyanobacteria, algae and higher plants, is at the heart of this process and it energizes the atmosphere with O_2. Photosystem II consists of 20 subunits with 17 trans-membrane and 3 extrinsic membrane proteins. The PSII also binds 35 chlorophylls, 2 pheophytins, 2 hemes, 1 non-heme iron, 2 plastoquinones (Q_A and Q_B), the Mn_4CaO_5 cluster, 2 Cl^-, 12 carotenoids and 25 lipids [1]. The light-induced electron transfer reactions start with the excitation of one of the chlorophylls of the antennae upon the absorption of a photon. The excitation is then transferred to the photochemical trap which consists of four chlorophylls, P_{D1}, P_{D2}, Chl_{D1}, Chl_{D2}. A charge separation then occurs resulting ultimately in the formation of the $Chl_{D1}^{+}Phe_{D1}^{-}$ and then in the $P_{D1}^{+}Phe_{D1}^{-}$ radical pair states, *e.g.* [2,3] for reviews. Then, P_{D1}^{+} oxidizes Tyr_Z, the Tyr161 of the D1 polypeptide, which in turn oxidizes the Mn_4CaO_5 cluster, *e.g.* [2] for a review. The electron on Phe_{D1}^{-} is then transferred to Q_A, the primary quinone electron acceptor and then to Q_B, the second quinone electron acceptor. Whereas Q_A can be only singly reduced under normal conditions, Q_B accepts two electrons and two protons before to leave its binding site, *e.g.* [4–6] and references therein.

The Mn_4CaO_5 cluster is oxidized by the oxidized Tyr_Z following each charge separation and cycles through five redox states denoted S_n, where *n* stands for the number of stored oxidizing equivalents. The S_1-state is stable in the dark so that S_1 is the preponderant state upon dark-adaptation. When the S_4-state is formed, *i.e.* after the 3rd flash of light given on dark-adapted PSII, the two water molecules bound to the cluster are oxidized, the O_2 is released and the S_0-state is reformed, *e.g.* [7–11] and references therein.

In the S_1-state, the refined structure of the crystallographic X-ray structure of the Mn_4O_5Ca [1,11] is like a distorted chair including a μ-oxo-bridged cuboidal Mn_3O_4Ca unit with a fourth Mn attached to this core structure *via* two μ-oxo bridges involving O4 and O5 [1]. Although

Abbreviations: PSII, Photosystem II; Chl, chlorophyll; MES, 2-(N-morpholino) ethanesulfonic acid; TAPS, N-[Tris(hydroxymethyl)methyl]-3-aminopropanesulfonic acid; P_{680}, primary electron donor; P_{D1} and P_{D2}, individual Chl on the D1 or D2 side, respectively, which constitute a pair of Chl with partially overlapping aromatic rings; Q_A, primary quinone acceptor; Q_B, secondary quinone acceptor; Phe, pheophytin; PPBQ, phenyl *p*–benzoquinone; EPR, Electron Paramagnetic Resonance; EDNMR, Electron Detected Nuclear Double Resonance; HS, high spin; LS, low spin; DFT, density functional theory; XFEL, X-ray free-electron laser; FTIR, Fourier transform infrared spectroscopy; NIR, near infrared

E-mail address: alain.boussac@cea.fr.

https://doi.org/10.1016/j.bbabio.2019.05.001
Received 17 February 2019; Received in revised form 10 April 2019; Accepted 1 May 2019
Available online 04 May 2019
0005-2728/

the structures of the Mn_4O_5Ca cluster in the S_2-state and S_3-state are expected to be resolved soon with a similar accuracy, the published structures [12,13] require improvements in $S_{2/3}$-state homogeneity, resolution and deconvolution. For the moment, the S_2 and S_3 structures rely in part on computations that are based on the X-ray free-electron laser structure of the S_1-state further restrained by data from X-ray spectroscopy and EPR spectroscopy, *e.g.* [11,14–26] for a non-exhaustive list of recent computational works.

The S_2-state exhibits, depending on the conditions, two different EPR signals detectable at helium temperatures. The first one has a low spin value $S = 1/2$, S_2^{LS}, characterized by a multiline signal made up of at least 20 lines separated by approximately 80 gauss, centered at $g \sim 2.0$ and spread over roughly 1800 gauss [27]. The second S_2-state configuration exhibits either a derivative-like signal centered at $g \sim 4.1$ [28,29] or more complex signals at lower magnetic fields, *i.e.* at higher g values, all attributed to high-spin ground states, S_2^{HS}, with $S \geq 5/2$, *e.g.* [30,31]. ENDOR analysis and X-ray spectroscopy of the S_2^{LS}-state indicate that the Mn_4CaO_5 contains one Mn^{III} ion and three Mn^{IV} ions [32,33].

From *in silico* works, it has been proposed that the S_2^{LS}-state and S_2^{HS}-state share almost the same coordination environment with the Mn^{III} ion located on Mn1 in the S_2^{LS}-state and on the Mn4 in the S_2^{HS}-state. This valence swap from Mn1 to Mn4 would also be associated with a moving of the oxygen O5 from a position where it links the Mn4, Mn3 and the Ca in the S_2^{LS} configuration to a position where it bridges the Mn1, Mn3 and Ca ions in the S_2^{HS} configuration thus resulting in a closed cubane structure [34]. These two configurations have been calculated as almost isoenergetic [35] as this is experimentally observed for the S_2^{LS}-state and S_2^{HS}-state [31,36].

The equilibrium between S_2^{LS} and S_2^{HS} has been recently shown to be pH dependent [37], with a $pK_a \sim 8.3$ for the native Mn_4CaO_5 and a $pK_a \sim 7.5$ for Mn_4SrO_5. DFT results suggested that exchanging Ca with Sr modifies the electronic structure of several titratable groups within the active site, including groups that are not direct ligands to Ca/Sr, *e.g.* W1/W2, D61, H332 and H337 [37].

The transition from the S_2^{LS}-state to states exhibiting high-spin EPR signals can also be induced by near-infrared (NIR) illumination at temperatures ≤ 150 K [31,38,39]. This effect is due to absorption of the IR light by the Mn_4-cluster itself but the photochemical process remains to be fully understood. It has been however recently proposed from a magnetic circular dichroism experiment that it could correspond to a spin-flip within the d^3 configuration of the Mn^{IV} ions in the cluster [40]. In a theoretical approach it has also been proposed [17] that NIR light induces, in a first step, a spin crossover in the S_2^{LS} open configuration in the $Mn1^{III}(\uparrow)$-$Mn2^{IV}(\downarrow)$-$Mn3^{IV}(\downarrow)$-$Mn4^{IV}(\uparrow)$ state resulting in an S_2^{HS} open configuration with a $Mn1^{III}(\downarrow)$-$Mn2^{IV}(\uparrow)$-$Mn3^{IV}(\uparrow)$-$Mn4^{IV}(\uparrow)$ spin arrangement. In a second step, there would be a $Mn1^{III}/Mn4^{IV}$ into $Mn1^{IV}/Mn4^{III}$ exchange together with a shift of O5 closing the cube and resulting into another S_2^{HS} configuration with the spin arrangement $Mn1^{IV}(\uparrow)$-$Mn2^{IV}(\uparrow)$-$Mn3^{IV}(\uparrow)$-$Mn4^{III}(\downarrow)$. This sequence would be in agreement with the two different S_2^{HS} EPR signals induced depending on the temperature at which the NIR illumination of plant PSII is given [30]. Indeed, NIR illumination at $T \leq 65$ K induces a state with the main resonances at $g \sim 10$ and 6 whereas at T ~ 150 K it induces the $g \sim 4.1$ state. The resonances at $g \sim 10$ and 6, induced by NIR illumination at $T \leq 65$ K, relaxes in the dark at 65 K $< T <$ 150 K into the $g \sim 4.1$ state. A logical consequence would be that resonances at $g \sim 10$ and 6 correspond to the S_2^{HS} open configuration with a $Mn1^{III}(\downarrow)$-$Mn2^{IV}(\uparrow)$-$Mn3^{IV}(\uparrow)$-$Mn4^{IV}(\uparrow)$ spin arrangement whereas formation of the $g \sim 4.1$ state with a closed configuration would only be possible at higher temperatures since its formation requires a more important structural rearrangement. All the states above which are populated by NIR illumination are potential intermediate states in the S_2^{LS} to S_3 transition.

From its X-band cw-EPR spectrum the S_3-state has been shown to have a spin $S = 3$ ground state [41]. A W-band and Q-band magnetic resonance spectroscopy study of this state showed that the four Mn ions of the cluster exhibit a Mn^{IV} formal oxidation state with an octahedral ligation sphere in an open cubane structure [42].

In the S_3-state, both near-infrared and visible illumination at helium temperatures result in the formation of a state exhibiting a split EPR signal [43–45] in 30–40% of the centers [46]. To explain this observation, it has been proposed that a photo-activation process resulted in the conversion of the Mn_4CaO_5 cluster into a state able to oxidize Tyr_Z and thus leading to the formation of a $(S_2Tyr_Z^{\cdot})$'-state at the expense of the S_3Tyr_Z-state [43]. However, the formation of the $(S_2Tyr_Z^{\cdot})$' split signal is not accompanied by a decrease of the $S = 3$ S_3 signal amplitude, *e.g.* [47], suggesting that the near-infrared photochemistry and the formation of the $S = 3$ signal does not occur in the same centers. Importantly, the action spectrum of the NIR effect is similar in S_2 and S_3 [39]. The NIR-induced conversion $S_3Tyr_Z \rightarrow (S_2^{HS}Tyr_Z^{\cdot})$' at 4.2 K suggests that these two states share structural similarities, *e.g.* [48], and it has been proposed that in S_3 the NIR light excites a d-d transition in a five-coordinated $Mn4^{IV}$ [49].

In addition to the oxidation of the Mn_4CaO_5 cluster in the S_2 to S_3 transition a proton is released into the bulk and a water molecule is proposed to bind to the Mn1 by different ways, *e.g.* [10,12,13,16,21,22,42,50–53]. All these make this transition very complex and it remains a major subject of debates, see [11] for an extensive discussion. For example, it has been proposed that only the S_2^{HS}-state was able to give an electron to $Tyr_Z^{\cdot}$ and therefore to progress to the S_3-state. In this model, the S_2^{LS} form of S_2 had therefore to be converted into the S_2^{HS} form in order to advance [24,54]. Always in this model, the S_2^{LS} to S_2^{HS} conversion would be triggered by the formation of $Tyr_Z^{\cdot}$ which would reorient of the dipole moment of the Mn_4CaO_5 cluster such that the locus of negative charge becomes directed towards W1, that is bound to Mn4, and its hydrogen bonding partner, D1-Asp61, resulting into the deprotonation of W1 [54]. Two experimental results support this model. Firstly, the kinetics of the proton release in the S_2 to S_3 transition is much faster [55–57], see however [58], than the electron transfer in the $S_2^{LS}Tyr_Z^{\cdot} \rightarrow S_3Tyr_Z$ transition and very likely occurs in the $S_2^{LS}Tyr_Z^{\cdot} \rightarrow S_2^{HS}Tyr_Z^{\cdot}$ intermediate step before the $S_2^{HS}Tyr_Z^{\cdot} \rightarrow S_3Tyr_Z$ transition happens [57]. Secondly, the temperature threshold at which the S_2^{LS} to S_3 transition is blocked at pH 6.5, that is ≈ 230–240 K [59], corresponds to the temperature at which the $S_2^{LS}Tyr_Z$ to $S_2^{HS}Tyr_Z$ transition is inhibited at high pH [47], a situation supposed to be close to that for $S_2^{LS}Tyr_Z^{\cdot}$ to $S_2^{HS}Tyr_Z^{\cdot}$ at pH 6.5 [57]. However, in contrast to the model above, Siegbahn rejected the closed cubane structure as an intermediate form in the S_2 to S_3 transition while suggesting instead that a high-spin configuration with an open cubane structure could be a transient state upon Tyr_Z oxidation [16].

In a DFT approach [34,35] the energy difference between the closed and open cubane configurations in S_2 has been calculated to be small. The closed cubane S_2 structure with a newly coordinated water molecule near the Mn4 site was also calculated more stable than the open cubane S_2 structure with a newly coordinated water molecule on the Mn1 site [60,61]. In contrast, in another computational work [16], the new water molecule is proposed to bind to Mn1 in a S_2^{HS} state with an open configuration at low pH values.

In the present work, the S_2 to S_3 transition has been further investigated, in relation with the different structures proposed for both S_2^{HS} and S_3, by following the temperature dependence of the S_2^{HS} to S_3 transition by EPR spectroscopy.

2. Materials and methods

2.1. Photosystem II preparation

Photosystem II was purified from a *Thermosynechococcus elongatus* *ΔpsbA$_1$ΔpsbA$_2$* deletion mutant that had a His_6-tag on the carboxy terminus of CP43 as previously described [62]. The purified PSII were

suspended in 1 M betaine, 15 mM $CaCl_2$, 15 mM $MgCl_2$, 40 mM MES, pH 6.5, then frozen in liquid nitrogen until use. For varying the pH values, PSII samples were washed by cycles of dilutions in 1 M betaine, 15 mM $CaCl_2$, 15 mM $MgCl_2$, followed by concentration using Amicon Ultra-15 centrifugal filter units (cut-off 100 kDa) until the estimated residual MES concentration was smaller than 1 μM. PSII samples were then loaded in the dark into quartz EPR tubes at 1.1 mg of Chl mL^{-1} and dark-adapted for 1 h at room temperature. The samples were then synchronized in the S_1-state with one pre-flash [63] given at room temperature. After a further 1 h dark-adaptation at room temperature the pH was adjusted to 8.6 by adding 100 mM, final concentration, of TAPS. This pH value was chosen because the EPR signals remain essentially unaffected until pH 9.0 and at pH 8.6 the high spin content is almost maximal [37]. After a further incubation in darkness for ~ 1 min at pH 8.6, the samples were frozen in the dark to 198 K. Prior to the recording of the first EPR spectrum, samples were degassed by pumping (~ 10^{-4} bar) at 198 K, filled with helium gas and the EPR tubes were then transferred into liquid nitrogen. All sample handling was done in darkness. When indicated, 0.5 mM PPBQ dissolved in dimethyl sulfoxide were added before the addition of TAPS.

2.2. EPR spectroscopy

X-band cw-EPR spectra were recorded with a Bruker Elexsys 500 X-band spectrometer equipped with a standard ER 4102 (Bruker) X-band resonator, a Bruker teslameter, an Oxford Instruments cryostat (ESR 900) and an Oxford ITC504 temperature controller. Flash illumination at room temperature was provided by a neodymium:yttrium–aluminum garnet (Nd:YAG) laser (532 nm, 550 mJ, 8 ns Spectra Physics GCR-230-10). Illumination at 198 K with visible light was done in a non-silvered Dewar filled with ethanol cooled with dry ice for approximately 5–10 s with a 800 W tungsten lamp filtered by water and infrared cut-off filters. For illumination at 77 K, the non-silvered Dewar was filled with liquid N_2. Illuminations at temperatures between 77 K and 198 K, were done in a nitrogen gas flow system (Bruker, B-VT-1000). Illumination at 4.2 K was done in the EPR cavity using a low-voltage halogen lamp (24 V, 250 W, Philips Type 13163) filtered by water and infrared cut-off filters. Near infrared (NIR) illumination was provided by a laser diode emitting at 813 nm (Coherent, diode S-81-1000C) with a power of 600–700 mW at the level of the sample. When mentioned, a warming of the samples was done in total darkness by plunging the EPR tubes in an ethanol bath at room temperature. Then, after approximately 5 s the PSII were refrozen as described above for dark-adapted samples.

3. Results

Firstly, control EPR experiments are reported in Figs. 1 to 4. Fig. 1 shows the results of either a one-flash illumination (Panels A and B) or a two-flash illumination (Panels C and D) given at room temperature to PSII samples at pH 8.6 in the absence of an added electron acceptor. The EPR spectra were recorded at either 4.2 K (Panels A and C) or 8.6 K (Panels B and D). Spectra a (in black) were recorded in dark-adapted samples and spectra b (in red) were recorded after the flash illumination. Spectra c (in blue) are the light-*minus*-dark difference spectra.

As previously reported [37], at pH 8.6 the one-flash illumination resulted in the formation of a S_2^{HS}-state characterized by an EPR signal centered at $g \sim 4.75$ (turning point at ~ 1425 gauss) in the great majority of PSII centers. The S_2^{HS} signal was detectable at both 4.2 K and 8.6 K (Panels A and C). The S_2-state in a low spin configuration (S_2^{LS}) and characterized by a multiline signal observable at 8.6 K and centered at $g \sim 2$ (~ 3400 gauss) was detected in a small minority of centers (Panel C). Upon the one-flash illumination, a broad signal at $g \sim 1.6$ (~ 4160 gauss) and a sharp peak at $g \sim 2.004$, better seen at 4.2 K, were also induced. These features originate from the biradical $Q_A^-Fe^{2+}Q_B^-$ magnetically coupled to the Fe^{2+} [5]. In our PSII samples, in the absence of an added artificial acceptor, Q_B^- is present in approximately half of the dark-adapted centers at pH 6.5 after a one hour dark-adaptation [4,6]. In spectra a, the $Fe^{2+}Q_B^-$ spin state exhibits the broad small signal between 3600 and 4800 gauss [5]. The detection of a $Q_A^-Fe^{2+}Q_B^-$ signal after a one flash-illumination and a two flash-illumination indicates that at pH 8.6 either one or both reactions $Q_A^-Fe^{2+}Q_B^- \rightarrow Q_AFe^{2+}Q_B^{2-} \rightarrow Q_AFe^{2+}Q_B + Q_BH_2$ are less efficient than at lower pH values. In agreement with this observation, the $Q_A^-Fe^{2+}Q_B^-$ signal has been shown to increase at high pH values in an experiment in which the samples were first illuminated at 198 K before being warmed to room temperature [37]. Finally, small negative signals were detected at $g \sim 5.65$ (~ 1200 gauss) and $g \sim 7.5$ (~ 900 gauss). These negative signals indicate that the non-heme iron was oxidized in a minor fraction of dark-adapted PSII samples and reduced by the flash illuminations as previously observed [6].

After illumination by two flashes (Panels B and D) the most intense feature of the S_3 signal at $g \sim 10$ (~ 680 gauss) [41] was detected at both 4.2 K and 8.6 K. Except the feature of the S_3 signal at 2300–2400 gauss which was also detected in Panel B and D, the other spectral signatures of the S_3-state were masked by the quinone signals, larger after 2 flashes than after one flash, and also by the S_2^{HS} signal because of the inevitable misses in flash experiments.

The presence of Q_B^- in a large fraction of centers together with a possible lower efficiency of the $Q_A^-Fe^{2+}Q_B^- \rightarrow Q_AFe^{2+}Q_B^{2-} \rightarrow Q_AFe^{2+}Q_B + Q_BH_2$ reactions at pH 8.6 prompted us to use an artificial electron acceptor in some experiments (*vide infra*). However, while the addition of an electron acceptor may increase the efficiency of multiple turnovers, it also increases the proportion of centers with an oxidized non-heme iron which gives an EPR signal that contributes to the EPR spectra [6,64]. The effect of the presence of PPBQ was tested at pH 8.6 in the experiment reported in Fig. 2. The spectra were recorded at 4.2 K (Panel A) and at 8.6 K (Panel B) in dark-adapted PSII samples (spectra a, black), after continuous illumination with visible light at 198 K (spectra b, red) and after warming for a few seconds at room temperature (spectra c, blue). Spectra d (green) and e (magenta) are the difference spectra b-*minus*-a and c-*minus*-a, respectively. As expected, no contribution from $Fe^{2+}Q_B^-$ is present in the dark spectra. Instead, the oxidized non-heme iron signal ($g \sim 5.65$ and $g \sim 7.5$) was larger than in the absence of PPBQ. As previously reported [37], the 198 K illumination induced the formation of the S_2^{LS} signal (spectra b and d) and no S_2^{HS} signal was detected. At 4.2 K, the multiline signal in the S_2^{LS}-state is saturated with the microwave power used and is therefore hardly detectable. The oxidized non-heme iron was reduced in the centers in which it was oxidized prior to the illumination and in the other centers the $Q_A^-Fe^{2+}$ signal at $g \sim 1.90$ (~ 3570 gauss) was induced [6]. The signal at $g \sim 1.6$ has no clear origin here except if we assume that two turnovers may occur under the short continuous illumination at 198 K. However, this does not seem the case because no oxidation of Cytb_{559}/Car/Chl/Tyr_D was observed (not shown but this is clear for Cytb_{559} in panel B) and no S_3 signal was induced (this is clear in spectra d). A double transition from S_0 to S_2 is also very unlikely because of the pre-flash protocol. Upon the warming of the sample (Fig. 2, spectra c and e), most of the centers in the S_2^{LS} configuration were converted into centers with a S_2^{HS} configuration as seen earlier for samples at this pH [37], thus showing no unexpected effect of PPBQ on this S_2^{LS} to S_2^{HS} conversion. The only effect of PPBQ upon the warming of the sample was a re-oxidation of the reduced quinones and consequently the re-oxidation of the non-heme iron by the $PPBQ^-$ formed [64].

The effect of NIR illumination at pH 8.6 was monitored both in the S_2^{HS}-state and S_3-state (Fig. 3). Spectrum a (in red) in Panel A was recorded at 4.2 K after 1 flash given at room temperature, *i.e.* in PSII with the great majority of centers in the S_2^{HS} configuration, see above and [37]. Spectrum b (in green) was recorded after a further NIR illumination given at 4.2 K. Spectrum c (in blue) is the difference spectrum b-*minus*-a, *i.e.* after-*minus*-before NIR illumination. Two observations can be made. Firstly, the NIR illumination induced the formation of a very small split signal around the g = 2 region (with peak and trough at

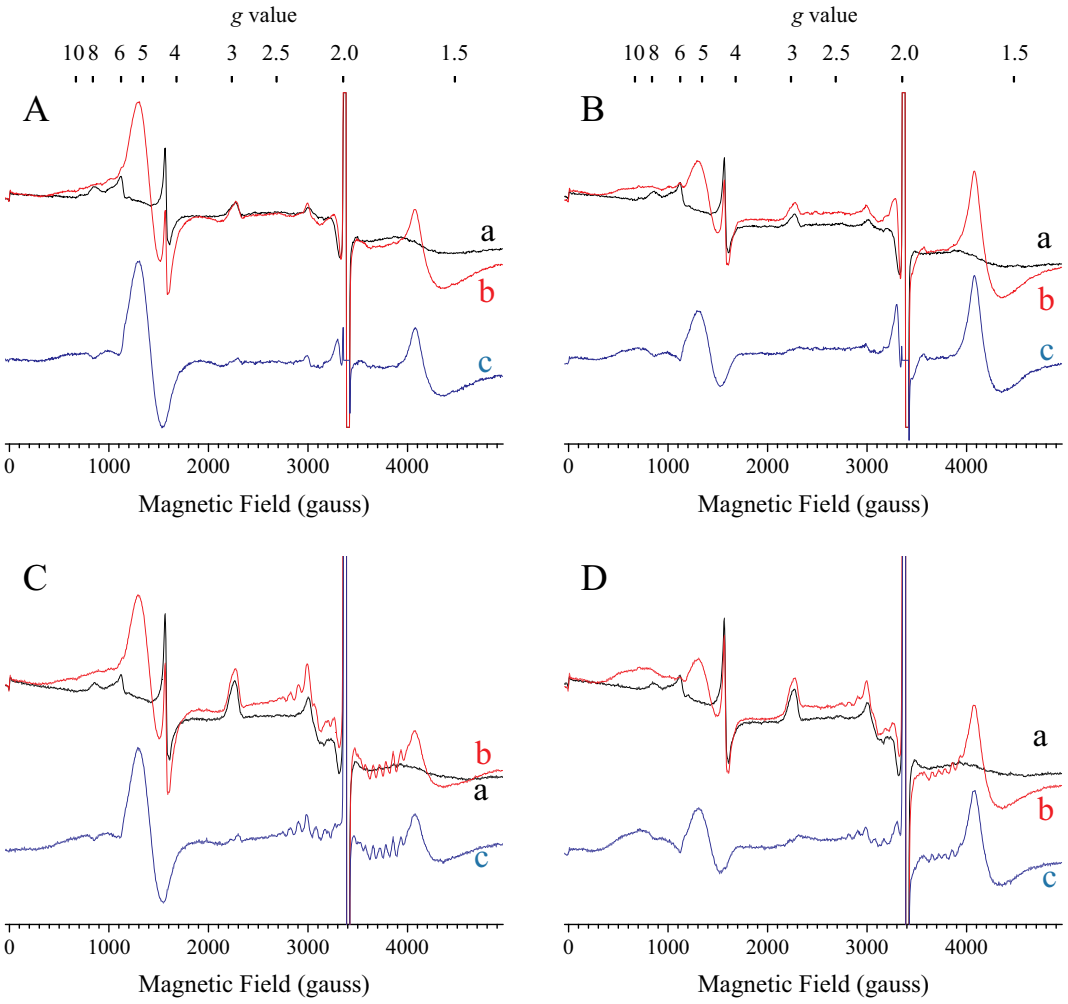

Fig. 1. EPR spectra at pH 8.6 recorded at 4.2 K (Panels A and B) and at 8.6 K (Panels C and D). The black spectra were recorded in dark-adapted PSII. The red spectra were recorded after one flash given at room temperature in Panels A and C and after two flashes given at room temperature in Panels B and D. The blue spectra are the "light"-*minus*-"dark" difference spectra *i.e.* the spectra recorded after the flash illuminations *minus* spectra recorded in the dark-adapted PSII. Instrument settings: [Chl] = 1.1 mg · ml^{-1}; modulation amplitude, 25 G; microwave power, 20 mW; microwave frequency, 9.4 GHz; modulation frequency, 100 kHz. The unresolved spectral region at $g \approx 2$ corresponds to the saturated signal from Tyr_D·. (For interpretation of the references to color in this figure legend, the reader is referred to the web version of this article.)

3304 and 3476 gauss, respectively), very likely originating from the NIR conversion of the residual S_2^{LS}-state into a S_1Tyr_Z·-state, as previously observed for such an illumination at 4.2 K [43,44,65]. However, the shape of this split signal observed here at pH 8.6 differs slightly from that observed at lower pH values [65]. Secondly, the major effect was an unexpected full conversion of the S_2^{HS} signal into another S_2^{HS} signal, which we will call $S_2^{HS'}$. The difference signal "after NIR-*minus*-0 flash" is shown in Panel B (spectrum d) with an expanded magnetic field scale and is compared to the S_2^{HS} signal observed in the V185T mutant [57] (spectrum e). The two spectra are remarkably similar thus suggesting a similar geometry for the Mn_4CaO_5 cluster in the $S_2^{HS'}$-state at pH 8.6 in the PsbA3-PSII and the S_2^{HS}-state at pH 6.5 in the V185T-PSII.

Because of the great sensitivity of the S_2^{HS}-state to the NIR light reported here (Fig. 3), it was not possible to monitor the effect of such a NIR illumination in the S_3-state generated by 2 flashes. Indeed, under these conditions there is a proportion of PSII in the S_2^{HS} configuration which remains present due to the photochemical misses (see Fig. 1B and D). To get around this problem, an experiment similar to that reported previously, in which the sample was subjected to a 198 K illumination and then to a series of warmings to room temperature and re-illuminations at 198 K [37], was carried out. Spectra in Fig. 4 were recorded at 4.2 K and the spectrum a (in black) was recorded from a dark-adapted sample, *i.e.* in the S_1-state. Spectrum b (in red) was recorded in a sample that was first illuminated at 198 K and then underwent four cycles of warming to room temperature followed by re-illumination at 198 K. Spectrum b exhibits the major feature of the S_3 signal at $g \sim 10$, that we designate here, $S_3^{S=3}$, and a small residual proportion of S_2^{HS} signal that was much less intense than after the 2-flash illumination as seen in Fig. 1B. Spectrum c (in blue) was then recorded after a NIR illumination at 4.2 K. The difference spectrum after-*minus*-before the NIR illumination (spectrum d, in green) exhibits an intense split signal and a low-field signal with a turning point at $g \sim 4.2$ (~ 1630 gauss). This low-field signal appeared free from contributions of the $S_2^{HS'}$ signal. Both the split signal and the low-field signal were hardly affected by the pH value between 5.5 and 7.5 (not shown but see [45] for the shape of the signal in this pH range) with, for the low-field signal, a turning point at $g \sim 4.5$ (~ 1520 gauss) and peak and trough positions at $g \sim 5.3$ and $g \sim 4.0$, respectively (not shown). The data in Fig. 4 shows that at pH 8.6 the NIR-induced signal in the S_3-state had a low field feature slightly modified with a turning point at $g \sim 4.2$ (~ 1630 gauss) and peak and trough positions at $g \sim 4.6$ and $g \sim 3.7$, respectively. In contrast, the split signal induced at pH 8.6 appeared very similar to the split signal induced at lower pH values. The spectra

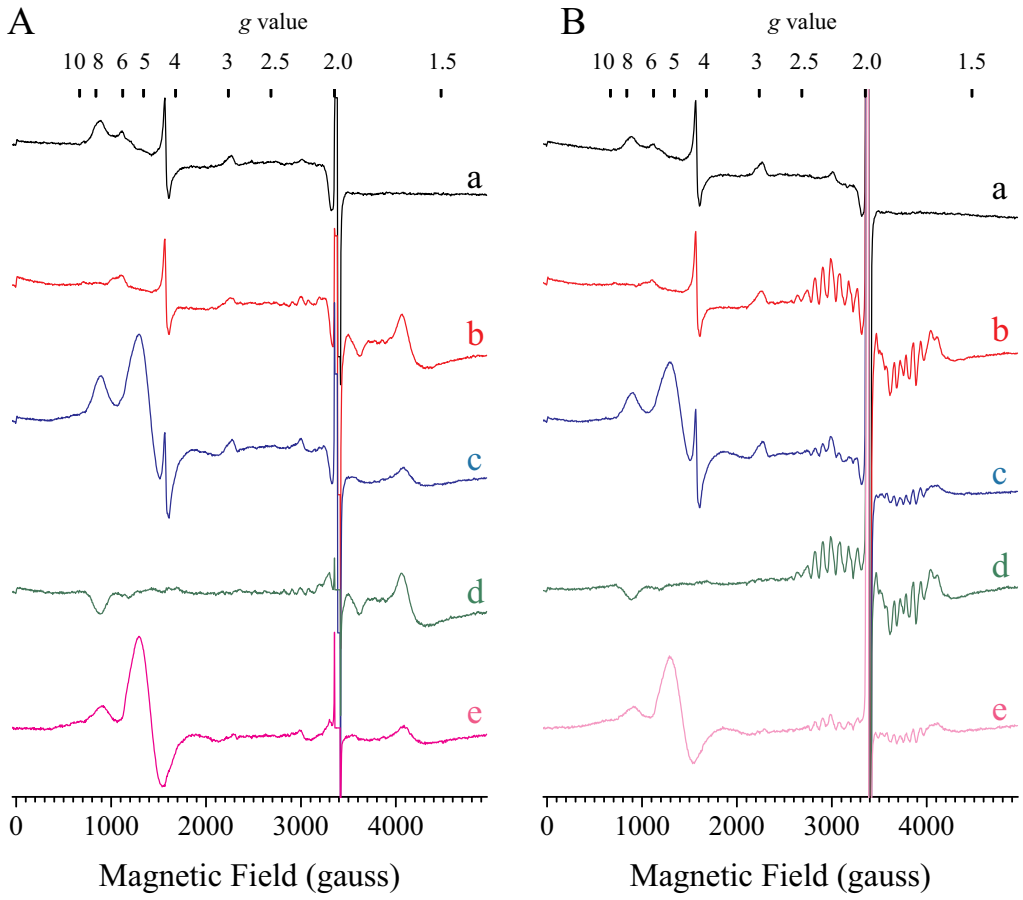

Fig. 2. EPR spectra at pH 8.6 recorded at 4.2 K (Panel A) and at 8.6 K (Panel B). Spectra a were recorded on dark-adapted PSII; Spectra b were recorded after continuous white light illumination at 198 K; Spectra c were recorded after a further warming at room temperature of the sample. Spectra d and e are the difference spectra spectrum b-*minus*-spectrum a and spectrum c-*minus*-spectrum a, respectively. Same instrument settings as in Fig. 1.

reported above also show that the quinone signal also appeared to be slightly sensitive to the NIR illumination (see also Fig. 3A). This effect, sometimes observed, will be investigated in a future work. The important point is that it will not affect the conclusions concerning the EPR of the Mn_4CaO_5 cluster that will be drawn from the present study since similar results were observed in the presence of PPBQ (not shown). In the light of the results in Figs. 1 to 4, we are now able to study the temperature dependence of the S_2^{HS} to S_3 transition.

The study of the S_2^{HS} to S_3 transition was done in the absence of PPBQ in order to get spectra free from contribution of the oxidized non-heme iron. The samples were first illuminated at 198 K to induce the S_2^{LS}-state. Then, the S_2^{LS}-state was converted into the S_2^{HS}-state by a brief warming of the sample, as in Fig. 2. The EPR spectra of the warmed samples were recorded before and after a second illumination with visible light at different temperatures from 198 K to 4.2 K. Fig. 5 shows these difference spectra after-*minus*-before the second illumination given at 198 K (a), 120 K (b), 105 K (c), 77 K (d). When the second illumination was given at 198 K (a) all the S_2^{HS} disappeared and the $S_3^{S=3}$ signal was formed, see also [37,47]. When the temperature was decreased, the proportion of centers in which the S_2^{HS} disappeared (signal centered at 1413 gauss) progressively decreased and the $S_3^{S=3}$ signal formed ($g \sim 10$, ~ 630 gauss) also decreased, becoming very small, although still detectable, at 77 K. The complication in the blue spectrum is that the negative signal between 600 and 1000 gauss due to the reduction of the non-heme iron signal was not negligible (despite the absence of PPBQ) when compared to the light-induced $S_3^{S=3}$ signal. The smaller amplitude of both the $S_3^{S=3}$ signal and the negative S_2^{HS} signal below 120 K could be due to a weaker efficiency of the charge separation since the quinone signals ($g \sim 1.6$) also significantly decreased. However, the important point here is that the S_2^{HS}-state can progress, at least in a proportion of centers, at 105 K and probably until 77 K, to a state that exhibits a similar feature to that observed in the EPR signal of the $S_3^{S=3}$-state generated by 2 flashes at room temperature. When the second illumination was performed at 77 K (d, blue spectrum) a small split signal seemed to be also induced (peak at $g \sim 2.06$, ~ 3290 gauss and trough at $g \sim 1.95$, ~ 3476 gauss). This will be discussed later on in this section.

The effects of an illumination of the S_2^{HS}-state were further investigated down to 4.2 K. In this experiment, PPBQ was added in order to have the acceptor side fully oxidized at the beginning of the experiment. Similar results were however obtained in the absence of PPBQ (not shown). Fig. 6 shows difference spectra recorded at 4.2 K and obtained by subtracting the spectrum previously recorded in the dark-adapted sample from that recorded after each of the steps. Spectrum a (in black) shows the changes induced by the 198 K illumination previously described in Fig. 2, with the formation of the quinone signals and the negative non-heme iron signal. Spectrum b (in red) shows the effects of the warming of the sample, *i.e.* the conversion of the S_2^{LS}-state, which is not detected at 4.2 K, into the S_2^{HS}-state, which is detectable at 4.2 K. The warming also allowed the PPBQ to re-oxidize the reduced quinones and consequently the non-heme iron to be re-oxidized by the $PPBQ^-$ formed. The sample was then illuminated by visible light at 4.2 K directly in the EPR cavity (c, blue spectrum). Two observations can be made. Firstly, the non-heme iron was reduced in the centers in which it was oxidized prior to the 4.2 K illumination and, in the other centers, the illumination induced a small increase of the quinone signal. Secondly, more than half of the S_2^{HS} signal disappeared and a split signal appeared. Thirdly, no $S_3^{S=3}$ signal was detected after the 4.2 K illumination. Several possibilities can be invoked to explain these results. In one hand, the illumination with visible light at 4.2 K results in an $S_2^{HS}Tyr_Z \rightarrow S_2^{HS}Tyr_Z^{\cdot}$ transition that would explain the formation of the split signal and the decrease of the S_2^{HS} signal. On the

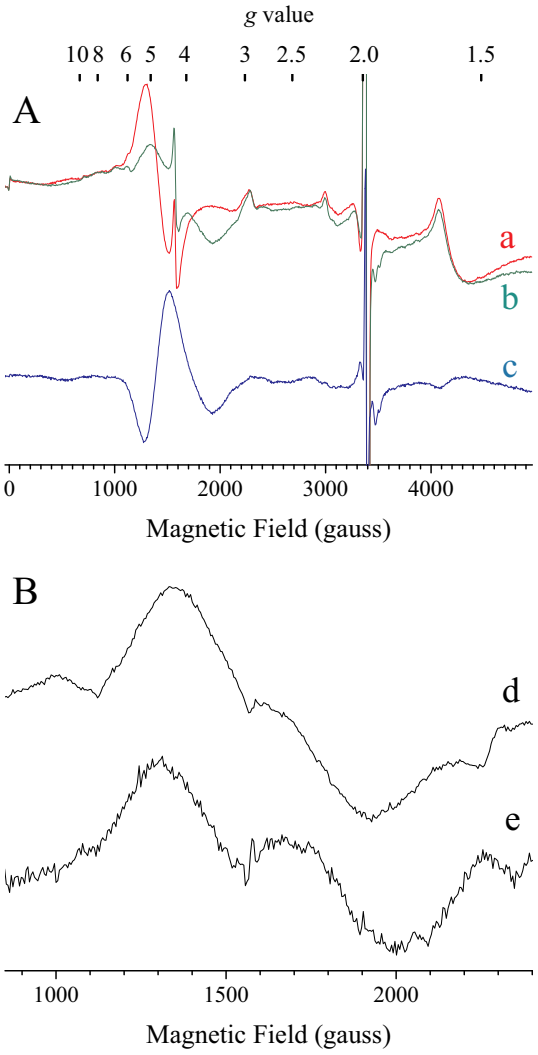

Fig. 3. EPR spectra at pH 8.6 recorded at 4.2 K. In Panel A, spectrum a was recorded after a warming of the sample at room temperature following the illumination at 198 K, spectrum b was recorded after a further NIR illumination at 4.2 K and spectrum c is the difference spectrum spectrum b-*minus*-spectrum a. Spectrum d in Panel B is the difference spectrum spectrum b-*minus*-the dark spectrum (*i.e.* spectrum a in Fig. 2A). Spectrum e in Panel B is the S_2^{HS} signal at pH 6.5 in the V185T mutant [57]. Same instrument settings as in Fig. 1.

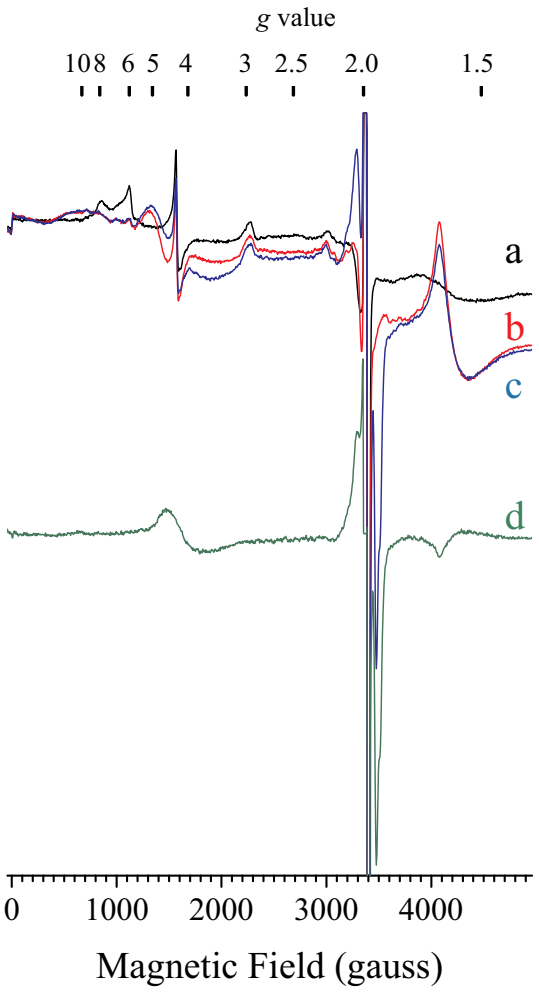

Fig. 4. EPR spectra at pH 8.6 recorded at 4.2 K. Spectrum a was recorded on a dark-adapted sample. Spectrum b was recorded in a sample that was first illuminated at 198 K and then underwent four cycles of warming to room temperature followed by re-illumination at 198 K. Spectrum c was recorded after a further NIR illumination at 4.2 K. Spectrum d is the difference spectrum spectrum c-*minus*-spectrum a. Same instrument settings as in Fig. 1.

other hand, a sequence with two events could explain these observations with first of all the formation of the EPR invisible S_3-state, S_3^{inv}, and subsequently the formation of a ($S_2Tyr_Z^{\bullet}$)'-state, responsible for the split signal, at the expense of the S_3^{inv}-state, as previously demonstrated at lower pH values in different PSII from plant and from a cyanobacterium (see the introduction section). A careful examination of spectrum c indicates a small negative feature at around 2000 gauss. This feature perfectly matches the $S_2^{HS'}$ signal induced by NIR-illumination of the S_2^{HS}-state (see Fig. 3B). This suggests that the S_2^{HS}-state is very likely also directly sensitive to the visible light in addition to its sensitivity to the NIR light. After a dark period (~ 10–20 min) at 4.2 K following the 4.2 K illumination, a new spectrum was recorded (d, in green). In spectrum d most of the split signal detected in spectrum c had disappeared. In contrast, the amplitude of both the low-field signals and the quinone signals remained almost unaffected. This observation argues against the reformation of the $S_2^{HS}Tyr_Z$-state present prior to the 4.2 K illumination from an $S_2Tyr_Z^{\bullet}$-state in a charge recombination process since, in the case of the charge recombination, the S_2^{HS} signal would be larger in spectrum d than in spectrum c and the quinone signals would be smaller in spectrum d than in spectrum c.

Finally, a spectrum was recorded under NIR light (e, magenta). The negative signal at 2000 gauss belonging to $S_2^{HS'}$ signal increased at the expense of the remaining S_2^{HS} signal as described in Fig. 3A and, more importantly, the split signal reappeared. This observation indicates that the S_3^{inv}-state was formed by the previous 4.2 K illumination in a fraction of centers. In other words, we can conclude that the S_3^{inv}-state, from which both NIR illumination and visible illumination can generate a ($S_2Tyr_Z^{\bullet}$)' split signal, can be formed from the S_2^{HS}-state at temperatures down to 4.2 K.

The spectrum of the NIR-induced state in Fig. 6 (spectrum e, magenta) was recorded under NIR illumination and not after the NIR illumination. This was necessary because we observed that the split signal induced by NIR illumination was not stable and decayed in the dark, in contrast to the situation in a 2-flash sample. The possibility that the $S_2^{HS}Tyr_Z \rightarrow S_3^{inv}Tyr_Z \rightarrow (S_2Tyr_Z^{\bullet})'$ also occurs at higher temperatures but with a shorter lifetime than at low temperatures for the ($S_2Tyr_Z^{\bullet}$)'-state cannot be discarded. In fact, this would explain why a split signal was detected up to 77 K but not above where the decay would be too fast (spectrum d in Fig. 5).

The last point investigated in the present study was which of the two high-spin states, S_2^{HS} or $S_2^{HS'}$, is able to progress to the S_3^{inv}-state, in a proportion of centers, when white light illumination is given at 4.2 K?

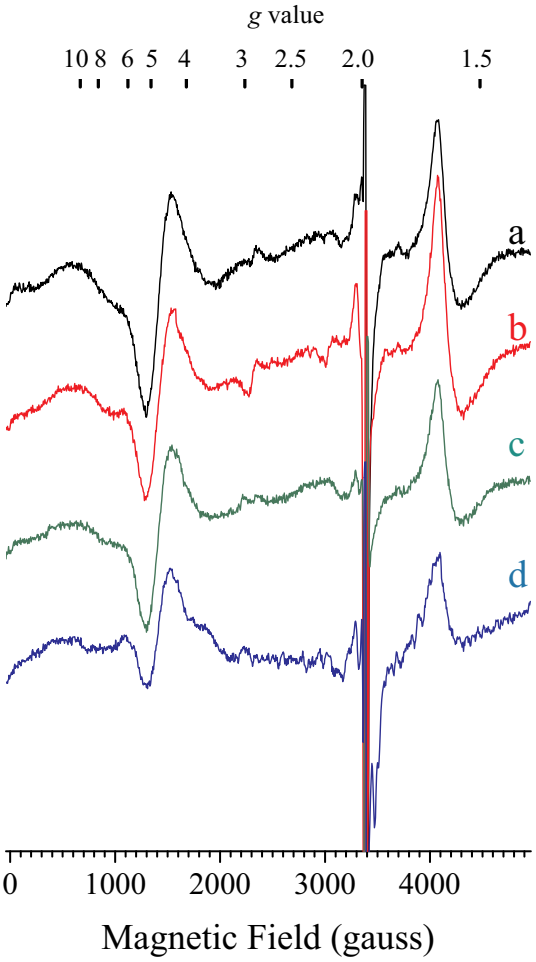

Fig. 5. EPR spectra at pH 8.6 recorded at 8.6 K. The sample was first illuminated at 198 K, then warmed a few seconds at room temperature and a second illumination at 198 K was given. The spectra shown are the difference spectra after-*minus*-before the second illumination given at 198 K (a), or 120 K (b), or 105 K (c) or 77 K (d). Same instrument settings as in Fig. 1.

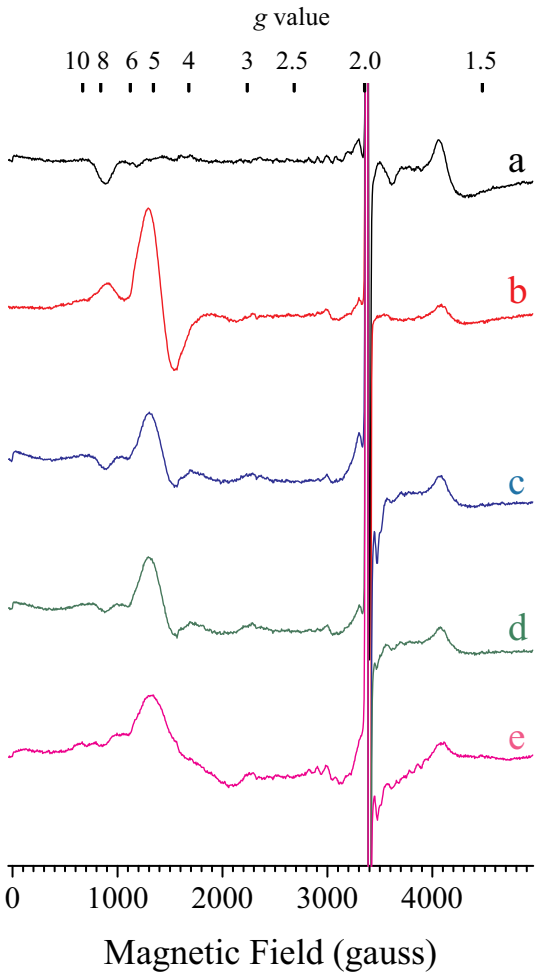

Fig. 6. EPR spectra at pH 8.6 recorded at 4.2 K. All spectra are difference spectra obtained by subtracting the spectrum previously recorded in the dark-adapted sample from that recorded after each of the steps. Spectrum a was recorded after an illumination at 198 K. Spectrum b was recorded after the warming of the sample. Spectrum c was recorded after a further white light illumination given at 4.2 K. Spectrum d was recorded after a dark-period (10–20 min) at 4.2 K. Spectrum e was recorded after a further NIR illumination at 4.2 K. Same instrument settings as in Fig. 1.

Two sequences of events could be proposed: either *i*) a direct oxidation of the S_2^{HS}-state, $S_2^{HS} \rightarrow S_3^{inv}$, or *ii*) a two-step sequence, $S_2^{HS} \rightarrow S_2^{HS'} \rightarrow S_3^{inv}$, in which a photochemical event at the level of the Mn_4CaO_5 cluster occurs first before the cluster is oxidized. Since the illumination at 4.2 K with both NIR light and visible light converts the S_2^{HS}-state into the $S_2^{HS'}$-state, it is impossible to conceive of a sequence of illuminations that would avoid the formation of the $S_2^{HS'}$-state as a possible intermediate state. However, the experiment reported in Fig. 7 allows us to determine whether the $S_2^{HS'}$-state can be an intermediate state between the S_2^{HS}-state and the S_3^{inv}-state or not. Panel A in Fig. 7 shows the spectra recorded at 4.2 K. Panel B shows the "spectrum from each successive treatment step-*minus*-dark" difference spectra obtained by subtracting the spectrum in the dark-adapted state (*i.e.* spectrum a in Panel A) from the spectra b to f in panel A. Panel C shows difference spectra in which successive spectra in Panel A are subtracted from each other, *i.e.* b-*minus*-a, c-*minus*-b, etc… Spectra b (in red) corresponds to the sample illuminated by 1 flash at room temperature in the presence of PPBQ, see Fig. 3A for a similar experiment. Spectra c (in blue) show the effect of NIR illumination at 4.2 K after the illumination by 1 flash. This NIR illumination, as explained above in Fig. 3A, converted the S_2^{HS}-state into a $S_2^{HS'}$-state. The sample was then further illuminated with visible light at 4.2 K. Spectra d (in magenta) were recorded under this white light illumination, and not after, for the reasons mentioned above, *i.e.* the light-induced signal was not stable and decayed back in the dark at 4.2 K. In spectra d, a large split signal was observed. In addition, the $S_2^{HS'}$-state disappeared (clearly visible in Panel C) and again no $S_3^{S=3}$ signal was detected. The electron acceptor was mainly the oxidized non-heme iron. Spectra e (in green) were obtained after incubation for a few seconds in the dark at 198 K. The split signal disappeared but the low-field signals remained unaffected although a careful inspection the spectrum in Panel C suggests that the signal at low-field that accompanied the split signal also disappeared. Then, the split signal could be re-induced by a NIR illumination at 4.2 K (spectrum f, in dark blue). Although this experiment is unable to tell us if the S_2^{HS}-state can progress directly to the S_3^{inv}-state at 4.2 K, it shows unambiguously that the $S_2^{HS'}$-state is able to do so.

4. Discussion

At pH values where the S_2^{LS}-state is the dominant state, it has been previously established that below 230 K the S_2^{LS}-state cannot progress beyond the $S_2^{LS}Tyr_Z^{\bullet}$-state, a state that exhibits a split EPR signal, *e.g.* [37]. It has been shown [57] that the $S_3^{S=3}$ signal is very similar, if not identical, in WT/Ca, WT/Sr, V185T/Ca and V185T/Sr *i.e.* four conditions in which the S_2-state exhibits different S_2^{LS}, different S_2^{HS} and different proportions of these two spin states. Therefore, since in WT/

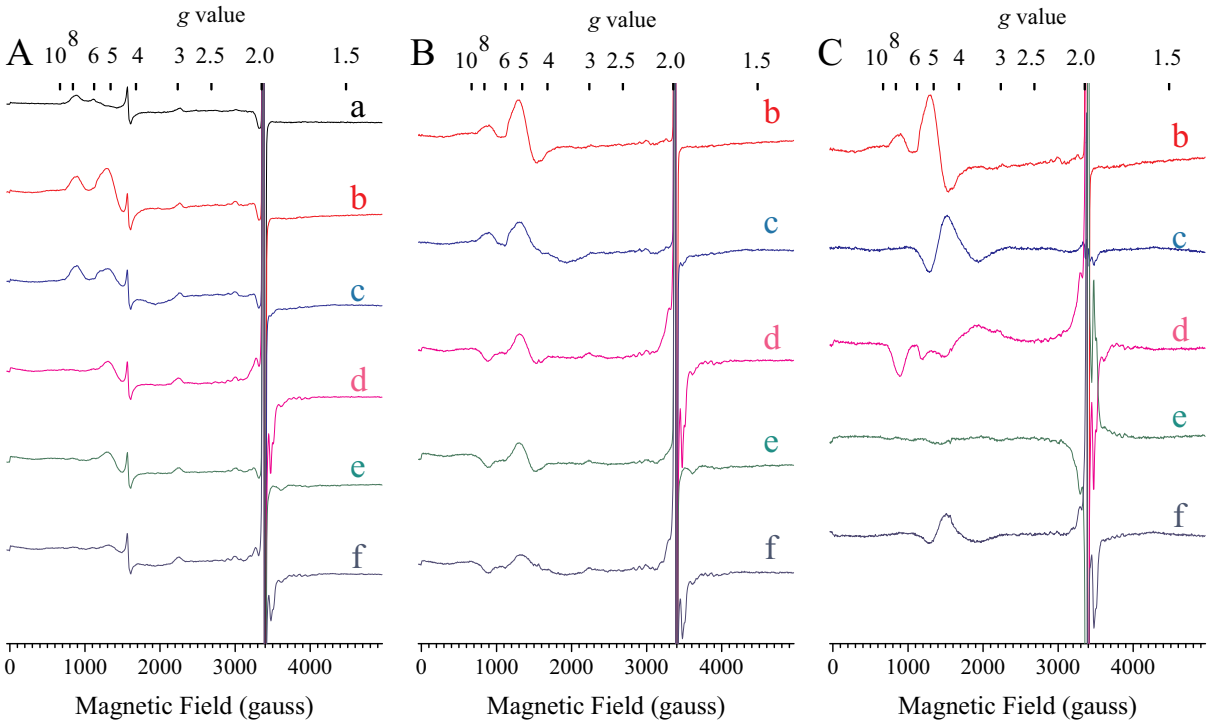

Fig. 7. EPR spectra at pH 8.6 at 4.2 K. Panel A shows the spectra recorded after each of the steps. Panel B shows the "the spectrum from each successive treatment step-*minus*-dark" difference spectra obtained by subtracting the spectrum in the dark-adapted state (*i.e.* spectrum a in Panel A) from the spectra b to f in panel A. Panel C shows difference spectra in which successive spectra in Panel A are subtracted from each other, *i.e.* b-*minus*-a, c-*minus*-b, *etc*. Spectra b corresponds to the sample illuminated by 1 flash at room temperature. Spectra c show the effect of a further NIR illumination given at 4.2 K. Spectra d were recorded under this white light illumination. Spectra e were obtained after incubation for a few seconds in the dark at 198 K. Spectrum f were recorded after a new NIR illumination at 4.2 K. Same instrument as in Fig. 1. Each panel have a different vertical scale.

Ca-PSII the starting and final states *i.e.* S_2^{LS} and $S_3^{S=3}$, respectively, are the same at low pH and high pH values, it seems likely that the changes observed depending on the pH value correspond to the trapping of intermediate states at different steps of the S_2^{LS} to $S_3^{S=3}$ transition. The EPR measurements in the present study focus on the light and temperature dependence of the S_2 to S_3 transition in *T. elongatus* PSII where the S_2^{HS}-state is the main S_2 configuration, *i.e.* at pH 8.6. This situation is expected to mimic the formation of $Tyr_Z^{\bullet}$ in the S_2-state at lower pH values [37]. Several observations have been made.

Firstly, the S_2^{HS}-state is sensitive to both NIR light and visible light, converting it at 4.2 K into a $S_2^{HS'}$-state that exhibits a slightly different EPR signal. Secondly, visible light illumination at 77 K advances the S_2^{HS}-state, in a fraction of centers, into a state exhibiting an EPR signal similar to that recorded after 2 flashes at room temperature, *i.e.* very likely into another $S_3^{S=3}$ state. Thirdly, in another proportion of centers, visible light illumination at 77 K advances the S_2^{HS}-state to form an S_3-state that lacks an EPR signal, S_3^{inv}, and this still occurs down to 4.2 K. Fourthly, this S_3^{inv}-state formed at 4.2 K is sensitive to both NIR and visible light, being converted into an $(S_2Tyr_Z^{\bullet})'$-state, which exhibits a split EPR signal very similar, although not identical, to the split signal induced by NIR light in the S_3^{inv}-state at pH 6.5 formed by two flashes at room temperature [45]. The $(S_2Tyr_Z^{\bullet})'$signal formed under these conditions is not stable at 4.2 K and decays back to the S_3^{inv}-state, in contrast to the behavior of the similar signal in the two-flash sample at pH 6.5. Fifthly, upon illumination at 4.2 K, $S_2^{HS'}$ can progress directly to the S_3^{inv}-state so that it is not possible to determine whether the photo-conversion of the S_2^{HS} into the S_3^{inv} occurs directly or *via* the $S_2^{HS'}$ intermediate. Given the considerable number of computational approaches concerning the S_2 to S_3 transition in the recent years, it is outside the scope of the present work to discuss all of them, see [11] for a more extensive review. Therefore, only major points will be discussed in view of several structural events occurring in this transition that are the preloading of water, the binding of water to the cluster, deprotonation steps and possible structural changes in the cluster.

Two of the issues under discussion are *i*) is an S_2^{HS}-state an (obligatory) intermediate state in the S_2 to S_3 transition and *ii*) what is the structure of this S_2^{HS}-state, *i.e.* open *versus* closed cubane configuration? In a recent work, Siegbahn [16] has revisited his previous publications and is now proposing that after the release of one proton from W1, following the oxidation of Tyr_Z, a series of intermediate reactions would result in a S_2 configuration with W3(OH^-) bound on Mn1 and W2(OH^-) and W1(H_2O) bound to Mn4 and that this S_2 intermediate is likely high-spin. However, in the same work [16], it is argued that a closed configuration is never involved in the S_2 to S_3 transition. So, there is still a contradiction with works in which the closed configuration is proposed to be the only one able to give an electron to $Tyr_Z^{\bullet}$, *e.g.* [17,24,35,54]. Starting from a closed configuration in S_2 to arrive in an S_3 open configuration with a new water bound on Mn1 has been proposed to occur, at room temperature, *via* either a pivot [49] or carousel [22] mechanism involving the water molecules bound to the Mn4. However, such mechanisms have also been rule out for energetic reasons in [16].

In several computational studies the S_3-state may exhibit several configurations in equilibrium at room temperature, *e.g.* [50], and 3 of them have been discussed in detail, *e.g.* [11]. The main one, derived from the study of the $S = 3$ EPR signal [42] and designated either $S_3^{A,W}$ in [11], or (*R*)-opened hydroxide in [18,50], is the S_3 configuration reached by two flashes at room temperature with an open configuration, a new water (OH^-) bound on Mn1, a di-μ-oxo bridge between Mn3 and Mn4 and W1(OH^-) and $W_{new}(H_2O)$ bound to Mn4. It seems rather unlikely that such a structure could be reached at temperatures as low as 77 K from a S_2^{HS} closed configuration as that one described in [34] due to the large structural reorganization which would be required. A second S_3 configuration, noted $S_3^{B,W}$ in [11], in equilibrium at

room temperature with $S_3^{A,W}$, has also been proposed. This structure has a closed configuration with only O4 bridging Mn3 and Mn4 and 3 water molecules bound to Mn4, $W_{new}(H_2O)$, W1(OH^-), W2(OH^-). It is moreover proposed that such a structure is expected to exhibit a $S = 3$ signal very similar to that from $S_3^{A,W}$ [11], in cw-EPR. Therefore, it seems possible that the $S_3^{B,W}$ state corresponds to the EPR signal detected at $g \sim 10$ upon 77 K illumination of the S_2^{HS}-state. However, although the structural changes in this model are less than those required to form the $S_3^{A,W}$ state when the starting state is a S_2^{HS}-state as defined in [34], a new water molecule should nevertheless bind to Mn4 and this also seems rather unlikely at 77 K. Alternatively, it is possible that W_{new} was already bound to Mn4 in the S_2^{HS}-state at pH 8.6. It was indeed already shown that the proton that is released in the S_2 to S_3 transition at pH 6.5, is very likely released in the $S_2^{LS}Tyr_Z^{\cdot} \rightarrow S_2^{HS}Tyr_Z^{\cdot}$ step, *i.e.* in the $S_2^{LS} \rightarrow S_2^{HS}$ transition induced by $Tyr_Z^{\cdot}$, and that increasing the pH to 8.6 had a similar effect to the oxidation of Tyr_Z [37]. So, it can be proposed that the high pH also favors the binding of W_{new} to Mn4 after (or concomitantly to) the release of one proton from W1. This would be in agreement with an FTIR study in which the movement of a water molecule located near $Tyr_Z^{\cdot}$ and to the Mn_4CaO_5 cluster was observed before the electron transfer occurred [58]. In DFT [52] and QM/MM studies [48], the additional water molecule has also been proposed to bind to the Mn4 in a transient closed configuration of the cluster in the $S_2Tyr_Z^{\cdot}$ state. In another QM/MM study [22] the insertion of the new water molecule in the S_2 to S_3 transition also occurs in a closed configuration. However, in this work [22], the final S_3 state remains in a closed configuration which is difficult to reconcile with the model proposed here.

An L-opened oxo structure with a O5-O6 distance equal to 2.43 Å and with a valence +4 for the 4 Mn has been also proposed to be EPR active with a spin $S = 3$ [18,50]. As in this structure the new water molecule is bound to Mn1 this would imply with the same reasoning as above that it is already bound in the S_2^{HS} state at high pH. In the computational approach done by Siegbahn [16] where there is no closed configuration involved in the S_2 to S_3 transition, the water molecule (W3 coming from the Ca site in this model) is already bound to Mn1 in the S_2^{HS}-state even at low pH values. In such a model, the S_3 state induced at 77 K from the S_2^{HS} state at pH 8.6 would be similar to that induced by two flashes at room temperature if we except probable small structural rearrangement around the cluster which are not possible at 77 K and which would be likely at the origin of the lower efficiency.

Experimentally, two transient states have been observed at 150 μs and 400 μs by XFEL spectroscopy after a flash given on PSII in the S_2^{LS} state *i.e.* in the time-range where the electron transfer from the Mn_4CaO_5 cluster to $Tyr_Z^{\cdot}$ occurs [13]. At 150 μs, *i.e.* much after the proton release ($t_{1/2}$ = 30 μs, [57]), Mn1 would move away from Mn4 by 0.2 Å. Then, at 400 μs, Ox becomes visible as a ligand to the Mn1 open coordination site with Ox being previously the W3 bound to Ca^{2+}. In computational works [18,50], a R-opened oxo intermediate with the intermediate O5-O6 distance equal to 2.21 Å and a +4 valence for the 4 Mn has been proposed to also be EPR active with a spin $S = 3$. Such a structure could be similar to that proposed in [13] for the structure detected at 400 μs. Although such intermediate could indeed exist, at 400 μs the S_2 to S_3 transition is fully completed in more than half of the centers and the detection of the intermediate states discussed here would require a measurement at times much shorter than 150 μs, *i.e.* when the great majority of centers are still in the $S_2Tyr_Z^{\cdot}$ state.

In the model proposed in [11] the Mn hyperfine coupling constants should differ in the $S_3^{B,W}$ and $S_3^{A,W}$ something that could deserve to be studied in future by redoing the ^{55}Mn-EDNMR measurements as in [42] on the $S_3^{S=3}$ signal generated at low temperature. The g value (~ 4.5) of the S_2^{HS} signal at pH 8.6 slightly differs from the S_2^{HS} signal (~ 4.1) previously simulated [34] and such a modification could result from the binding of W_{new} on Mn4 at pH 8.6. Testing this hypothesis by ^{55}Mn-EDNMR measurements is however not possible because the S_2^{HS} EPR signal has too fast relaxation properties. Vibrational spectroscopies like FTIR could be an alternative approach.

The S_3^{inv}-state which is NIR sensitive can be formed down to 4.2 K. If we refer again to the model in [11], this state would be analogous to the S_3^B state, described as possibly EPR silent, in which there is a closed cubane with W_{new} not yet bound. Of the three S_3 structures, $S_3^{A,W}$, $S_3^{B,W}$ and S_3^B, the latter is the closest to the S_2^{HS} simulated structure [34]. So, this would not be surprising that the $S_2^{HS}Tyr_Z^{\cdot} \rightarrow S_3^BTyr_Z$ reaction may occur until 4.2 K since the proton is already released during the S_2^{LS} to S_2^{HS} transition induced by increasing the pH. A S_3-state with a five-coordinated $Mn4^{IV}$ has been estimated as probably too high in energy to be involved in the S_2 to S_3 transition [66]. However, it remains uncertain if such conclusion could be affected by talking into account all the amino residues surrounding the cluster in the different spheres of coordination.

There is a probability that > 3 S_3-states are in equilibrium at room temperature [50]. However, the 3 structures $S_3^{A,W}$, $S_3^{B,W}$ and S_3^B seem enough to explain the data reported here. The other S_3 configurations could be transient states between the 3 states identified and discussed here. As discussed above, in our experiments we cannot distinguished the $S_3^{A,W}$ state formed at room temperature from the $S_3^{B,W}$ state that can be formed until 77 K. In ~ 60% of centers, a simple model for the sequence of events at room temperature would be: $S_2^{HS}Tyr_Z^{\cdot} \rightarrow S_3^{B,W}Tyr_Z \rightarrow S_3^{A,W}Tyr_Z$. The first step would occur down to 77 K and at room temperature there would be an equilibrium in favor of $S_3^{A,W}$ *via* a relaxation process, such as a change in the H-bond network. In the other ~ 40% of centers, the reaction would be $S_2^{HS}Tyr_Z^{\cdot} \rightarrow S_3^BTyr_Z$. The S_3^B state would be functional for O_2 evolution. Indeed, after 3 flashes the NIR-induced split signal attributed to the ($S_2Tyr_Z^{\cdot}$)'-state is much less intense than after two flashes (not shown, see also [44]). This means that either the S_3^B state is a functional state which can be oxidized by $Tyr_Z^{\cdot}$ or the conversion of the S_3^B state into the $S_3^{A,W}$ state is also triggered by the formation of $Tyr_Z^{\cdot}$. This model implies a heterogeneity in the S_2^{HS} configuration that does not seem to translate into different EPR signals as it seems unlikely they would have escaped detection. However, there is a precedence where a heterogeneity is difficult to detect. Indeed, in the S_2^{LS}-state, the centers susceptible to NIR light and those which are not exhibit multiline signals which only slightly differ [67]. The origin of this heterogeneity therefore remains difficult to identify but it is evident that there are a huge number of possibilities due to the high number of small adjustments in the H-bond network, for example, in the environment of cluster. In the case of the Siegbahn model [16] there would be only one EPR detectable S_3-state that could be formed at temperatures as low as 77 K and the sequence of events would be $S_2^{HS}Tyr_Z^{\cdot} \rightarrow S_3Tyr_Z$ with the binbing of W3 to Mn1 in the $S_2^{HS}Tyr_Z^{\cdot}$ at low pH values.

In conclusion, in this work and in the previous one [37], the experimental results support the involvement of the S_2^{HS} configuration as a transient state in the $S_2^{LS} \rightarrow S_3$ transition. The existence of a heterogeneity in S_3 [11,50] is experimentally supported and the different S_3-states experimentally observed could be intermediate states in the S_n-state cycle. The formation of one of these S_3-states, which is supposed to have a structure with the water molecule normally inserted in S_2 to S_3 transition at temperatures as low as 77 K, suggests that this water molecule is already bound in the S_2^{HS} state at pH 8.6 prior to the freezing of the sample. Assuming that increasing the pH to 8.6 mimics the formation of $Tyr_Z^{\cdot}$, as previously discussed [37], it is proposed that, at pH 6.5, the proton release [57], the S_2^{LS} to S_2^{HS} conversion [37] and the binding of the water molecule are all triggered by the formation of $Tyr_Z^{\cdot}$ in the S_2 to S_3 transition.

Transparency document

The Transparency document associated this article can be found, in online version.

Acknowledgements

Bill Rutherford and Miwa Sugiura are acknowledged for discussions and continuous supports. This work has been in part supported by the French Infrastructure for Integrated Structural Biology (FRISBI) ANR-10-INBS-05 and the ANR contract ANR-15PS2FIRX.

References

[1] M. Suga, F. Akita, K. Hirata, G. Ueno, H. Murakami, Y. Nakajima, T. Shimizu, K. Yamashita, M. Yamamoto, H. Ago, J.-R. Shen, Native structure of photosystem II at 1.95 angstrom resolution viewed by femtosecond X-ray pulses, Nature 517 (2015) 99–103.
[2] T. Cardona, A. Sedoud, N. Cox, A.W. Rutherford, Charge separation in photosystem II: a comparative and evolutionary overview, Biochim. Biophys. Acta 1817 (2012) 26–43.
[3] E. Romero, V.I. Novoderezhkin, R. van Grondelle, Quantum design of photosynthesis for bio-inspired solar-energy conversion, Nature 543 (2017) 355–365.
[4] C. Fufezan, C.-X. Zhang, A. Krieger-Liszkay, A.W. Rutherford, Secondary quinone in photosystem II of *Thermosynechococcus elongatus*: Semiquinone-iron EPR signals and temperature dependence of electron transfer, Biochemistry 44 (2005) 12780–12789.
[5] A. Sedoud, N. Cox, M. Sugiura, W. Lubitz, A. Boussac, A.W. Rutherford, The semiquinone-iron complex of photosystem II: EPR signals assigned to the low field edge of the ground state doublet of $Q_A \cdot {}^{-}Fe^{2+}$ and $Q_B \cdot {}^{-}Fe^{2+}$, Biochemistry 50 (2011) 6012–6021.
[6] A. Boussac, M. Sugiura, F. Rappaport, Probing the quinone binding site of photosystem II from *Thermosynechococcus elongatus* containing either PsbA1 or PsbA3 as the D1 protein through the binding characteristics of herbicides, Biochim. Biophys. Acta 1807 (2010) 119–129.
[7] J. Yano, V. Yachandra, Mn4Ca cluster in photosynthesis: where and how water is oxidized to dioxygen, Chem. Rev. 114 (2014) 4175–4205.
[8] J.-R. Shen, The structure of photosystem II and the mechanism of water oxidation in photosynthesis, Annu. Rev. Plant Biol. 66 (2015) 23–48.
[9] H. Dau, I. Zaharieva, M. Haumann, Recent developments in research on water oxidation by photosystem II, Curr. Opin. Chem. Biol. 16 (2012) 3–10.
[10] D.J. Vinyard, G.W. Brudvig, Progress toward a molecular mechanism of water oxidation in photosystem II, Annu. Rev. Phys. Chem. 68 (2017) 101–116.
[11] D.A. Pantazis, Missing pieces in the puzzle of biological water oxidation, ACS Catal. 8 (2018) 9477–9507.
[12] M. Suga, F. Akita, M. Sugahara, M. Kubo, Y. Nakajima, T. Nakane, K. Yamashita, Y. Umena, M. Nakabayashi, T. Yamane, T. Nakano, M. Suzuki, T. Masuda, S. Inoue, T. Kimura, T. Nomura, S. Yonekura, L.J. Yu, T. Sakamoto, T. Motomura, J.H. Chen, Y. Kato, T. Noguchi, K. Tono, Y. Joti, T. Kameshima, T. Hatsui, E. Nango, R. Tanaka, H. Naitow, Y. Matsuura, A. Yamashita, M. Yamamoto, O. Nureki, M. Yabashi, T. Ishikawa, S. Iwata, J.-R. Shen, Light-induced structural changes and the site of O=O bond formation in PSII caught by XFEL, Nature 543 (2017) 131–135.
[13] J. Kern, R. Chatterjee, I.D. Young, F.D. Fuller, L. Lassalle, M. Ibrahim, S. Gul, T. Fransson, A.S. Brewster, R. Alonso-Mori, R. Hussein, M. Zhang, L. Douthit, C. de Lichtenberg, M.H. Cheah, D. Shevela, J. Wersig, I. Seuffert, D. Sokaras, E. Pastor, C. Weninger, T. Kroll, R.G. Sierra, P. Aller, A. Butryn, A.M. Orville, M. Liang, A. Batyuk, J.E. Koglin, S. Carbajo, S. Boutet, N.W. Moriarty, J.M. Holton, H. Dobbek, P.D. Adams, U. Bergmann, N.K. Sauter, A. Zouni, J. Messinger, J. Yano, V.K. Yachandra, Structures of the intermediates of Kok's photosynthetic water oxidation clock, Nature 563 (2018) 421–425.
[14] P.E.M. Siegbahn, Water oxidation mechanism in photosystem II, including oxidations, proton release pathways, O-O bond formation and O2 release, Biochim. Biophys. Acta 1827 (2013) 1003–1019.
[15] X.C. Li, P.E.M. Siegbahn, U. Ryde, Simulation of the isotropic EXAFS spectra for the S-2 and S-3 structures of the oxygen evolving complex in photosystem II, Proc. Natl. Acad. Sci. U. S. A. 112 (2015) 3979–3984.
[16] P.E.M. Siegbahn, The S2 to S3 transition for water oxidation in PSII (photosystem II), revisited, Phys. Chem. Chem. Phys. 20 (2018) 22926–22931.
[17] K. Yamaguchi, H. Isobe, M. Shoji, S. Yamanaka, M. Okumura, Theory of chemical bonds in metalloenzymes XX: magneto-structural correlations in the CaMn4O5 cluster in oxygen-evolving complex of photosystem II, Mol. Phys. 114 (2016) 519–546.
[18] M. Shoji, H. Isobe, S. Yamanaka, Y. Umena, K. Kawakami, N. Kamiya, K. Yamaguchi, Theoretical elucidation of geometrical structures of the CaMn4O5 cluster in oxygen evolving complex of photosystem II scope and applicability of estimation formulae of structural deformations via the mixed-valence and Jahn-Teller effects, Adv. Quant. Chem. 78 (2019) 307–451.
[19] W. Ames, D.A. Pantazis, V. Krewald, N. Cox, J. Messinger, W. Lubitz, F. Neese, Theoretical evaluation of structural models of the S2 state in the oxygen evolving complex of photosystem II: protonation states and magnetic interactions, J. Am. Chem. Soc. 133 (2011) 19743–19757.
[20] V. Krewald, M. Retegan, N. Cox, J. Messinger, W. Lubitz, S. DeBeer, F. Neese, D.A. Pantazis, Metal oxidation states in biological water splitting, Chem. Sci. 6 (2015) 1676–1695.
[21] I. Ugur, A.W. Rutherford, V.R.I. Kaila, Redox-coupled substrate water reorganization in the active site of photosystem II-the role of calcium in substrate water delivery, Biochim. Biophys. Acta 1857 (2016) 740–748.
[22] J. Wang, M. Askerka, G.W. Brudvig, V.S. Batista, Crystallographic data support the carousel mechanism of water supply to the oxygen-evolving complex of photosystem II, ACS Energy Lett. (10) (2017) 2299–2306.
[23] A. Robertazzi, A. Galstyan, E.W. Knapp, Reprint of PSII manganese cluster: protonation of W2, 05, 04 and His337 in the S1 state explored by combined quantum chemical and electrostatic energy computations, Biochim. Biophys. Acta 1837 (2014) 1389–1394.
[24] D. Narzi, D. Bovi, L. Guidoni, Pathway for Mn-cluster oxidation by tyrosine-Z in the S2 state of photosystem II, Proc. Nat. Aca. Sci. USA 111 (2014) 8723–8728.
[25] D. Narzi, M. Capone, D. Bovi, L. Guidoni, Evolution from S-3 to S-4 states of the oxygen-evolving complex in photosystem II monitored by quantum mechanics/molecular mechanics (QM/MM) dynamics, Chem. Eur. J. 24 (2018) 10820–10828.
[26] Y. Guo, H. Li, L.L. He, D.X. Zhao, L.D. Gong, Z.Z. Yang, Theoretical reflections on the structural polymorphism of the oxygen-evolving complex in the S-2 state and the correlations to substrate water exchange and water oxidation mechanism in photosynthesis, Biochim. Biophys. Acta 1858 (2017) 833–846.
[27] G.C. Dismukes, Y. Siderer, Intermediates of a polynuclear manganese center involved in photosynthetic oxidation of water, Proc. Natl. Acad. Sci. U. S. A. 78 (1981) 274–278.
[28] J.-L. Zimmermann, A.W. Rutherford, Electron paramagnetic resonance studies of the oxygen-evolving enzyme of Photystem II, Biochim. Biophys. Acta 767 (1984) 160–167.
[29] J.L. Casey, K. Sauer, Electron paramagnetic resonance detection of a cryogenically photogenerated intermediate in photosynthetic oxygen evolution, Biochim. Biophys. Acta 767 (1984) 21–28.
[30] A. Boussac, S. Un, O. Horner, A.W. Rutherford, High spin states (S ≥ 5/2) of the photosystem II manganese complex, Biochemistry 37 (1998) 4001–4007.
[31] A. Boussac, H. Kuhl, S. Un, M. Rögner, A.W. Rutherford, Effect of near-infrared light on the S_2-state of the manganese complex of photosystem II from *Synechococcus elongatus*, Biochemistry 37 (1998) 8995–9000.
[32] J.M. Peloquin, K.A. Campbell, D.W. Randall, M.A. Evanchik, V.L. Pecoraro, W.H. Armstrong, R.D. Britt, Mn-55 ENDOR of the S-2-state multiline EPR signal of photosystem II: implications on the structure of the tetranuclear Mn cluster, J. Am. Chem. Soc. 122 (2000) 10926–10942.
[33] N. Cox, L. Rapatskiy, J.-H. Su, D.A. Pantazis, M. Sugiura, L. Kulik, P. Dorlet, A.W. Rutherford, F. Neese, A. Boussac, W. Lubitz, J. Messinger, The effect of Ca^{2+}/Sr^{2+} substitution on the electronic structure of the oxygen-evolving complex of photosystem II: a combined multi-frequency EPR, 55Mn-ENDOR and DFT study of the S_2 state, J. Am. Chem. Soc. 133 (2011) 3635–3648.
[34] D.A. Pantazis, W. Ames, N. Cox, W. Lubitz, F. Neese, Two interconvertible structures that explain the spectroscopic properties of the oxygen-evolving complex of photosystem II in the S_2 state, Angew. Chem. Intl. Ed. 51 (2012) 9935–9940.
[35] D. Bovi, D. Narzi, L. Guidoni, The S_2 state of the oxygen-evolving complex of photosystem II explored by QM/MM dynamics: spin surfaces and metastable states suggest a reaction path towards the S_3 state, Angew. Chem. Intl. Ed. 52 (2013) 11744–11749.
[36] D.J. Vinyard, S. Khan, M. Askerka, V.S. Batista, G.W. Brudvig, Energetics of the S-2 state spin isomers of the oxygen-evolving complex of photosystem II, J. Phys. Chem. B 121 (2017) 1020–1025.
[37] A. Boussac, I. Ugur, A. Marion, M. Sugiura, V.R.I. Kaila, A.W. Rutherford, The low spin - high spin equilibrium in the S_2-state of the water oxidizing enzyme, Biochim. Biophys. Acta 1859 (2018) 342–356.
[38] A. Boussac, J.-J. Girerd, A.W. Rutherford, Conversion of the spin-state of the manganese complex in photosystem II induced by near-infrared light, Biochemistry 35 (1996) 6984–6989.
[39] A. Boussac, M. Sugiura, D. Kirilovsky, A.W. Rutherford, Near-infrared-induced transitions in the manganese cluster of photosystem II: action spectra for the S_2 and S_3 redox states, Plant Cell Physiol. 46 (2005) 837–842.
[40] J. Morton, M. Chrysina, V.S.J. Craig, F. Akita, Y. Nakajima, W. Lubitz, N. Cox, J.-R. Shen, E. Krausz, Structured near-infrared magnetic circular dichroism spectra of the Mn_4CaO_5 cluster of PSII in *T. vulcanus* are dominated by Mn(IV) d-d 'spinflip' transitions, Biochim. Biophys. Acta 1859 (2018) 88–98.
[41] A. Boussac, M. Sugiura, A.W. Rutherford, P. Dorlet, Complete EPR spectrum of the S_3-state of the oxygen-evolving photosystem II, J. Am. Chem. Soc. 131 (2009) 5050–5051.
[42] N. Cox, M. Retegan, F. Neese, D.A. Pantazis, A. Boussac, W. Lubitz, Electronic structure of the oxygen evolving complex in photosystem II prior to O-O bond formation, Science 345 (2014) 804–808.
[43] V. Petrouleas, D. Koulougliotis, N. Ioannidis, Trapping of metalloradical intermediates of the S-states at liquid helium temperatures. Overview of the phenomenology and mechanistic implications, Biochemistry 44 (2005) 6723–6728.
[44] K.G.V. Havelius, J. Sjöholm, F.M. Ho, F. Mamedov, S. Styring, Metalloradical EPR signals from the $Y_Z \cdot$ S-state intermediates in photosystem II, Appl. Magn. Reson. 37 (2010) 151–176.
[45] A. Boussac, M. Sugiura, T.-L. Lai, A.W. Rutherford, Low-temperature photochemistry in photosystem II from *Thermosynechococcus elongatus* induced by visible and near-infrared light, Phil. Trans. R. Soc. B 363 (2008) 1203–1210.
[46] F. Rappaport, N. Ishida, M. Sugiura, A. Boussac, Ca^{2+} determines the entropy changes associated with the formation of transition states during water oxidation by photosystem II, Energy Environ. Sci. 4 (2011) 2520–2524.
[47] A. Boussac, A.W. Rutherford, M. Sugiura, Electron transfer pathways from the S_2-states to the S_3-states either after a Ca^{2+}/Sr^{2+} or a Cl^{-}/I^{-} exchange in photosystem II from *Thermosynechococcus elongatus*, Biochim. Biophys. Acta 1847 (2015) 576–586.
[48] M. Shoji, H. Isobe, T. Nakajima, Y. Shigeta, M. Suga, F. Akita, J.-R. Shen, K. Yamaguchi, Large-scale QM/MM calculations of the $CaMn_4O_5$ cluster in the S_3 state of the oxygen evolving complex of photosystem II. Comparison between

water-inserted and no water-inserted structures, Faraday Discuss. 198 (2017) 83–106.
[49] M. Retegan, V. Krewald, F. Mamedov, F. Neese, W. Lubitz, N. Cox, D.A. Pantazis, A five-coordinate Mn(IV) intermediate in biological water oxidation: spectroscopic signature and a pivot mechanism for water binding, Chem. Sci. 7 (2016) 72–84.
[50] M. Shoji, H. Isobe, K. Miyagawa, K. Yamaguchi, Possibility of the right-opened Mn-oxo intermediate (R-oxo(4444)) among all nine intermediates in the S_3 state of the oxygen-evolving complex of photosystem II revealed by large-scale QM/MM calculations, Chem. Phys. 518 (2019) 81–90.
[51] N. Cox, J. Messinger, Reflections on substrate water and dioxygen formation, Biochim. Biophys. Acta 1827 (2013) 1020–1030.
[52] M. Capone, D. Narzi, D. Bovi, L. Guidoni, Mechanism of water delivery to the active site of photosystem II along the S_2 to S_3 transition, J. Phys. Chem. Lett. 7 (2016) 592–596.
[53] C.J. Kim, R.J. Debus, Evidence from FTIR difference spectroscopy that a substrate H_2O molecule for O_2 formation in photosystem II is provided by the Ca ion of the catalytic Mn_4CaO_5 cluster, Biochemistry 56 (2017) 2558–2570.
[54] M. Retegan, N. Cox, W. Lubitz, F. Neese, D.A. Pantazis, The first tyrosyl radical intermediate formed in the S_2-S_3 transition of photosystem II, Phys. Chem. Chem. Phys. (2014) 11901–11910.
[55] F. Rappaport, M. Blanchard-Desce, J. Lavergne, Kinetics of electron-transfer and electrochromic change during the redox transitions of the photosynthetic oxygen-evolving complex, Biochim. Biophys. Acta 1184 (1994) 178–192.
[56] I. Zaharieva, H. Dau, M. Haumann, Sequential and coupled proton and electron transfer events in the $S_2 \rightarrow S_3$ transition of photosynthetic water oxidation revealed by time-resolved X-ray absorption spectroscopy, Biochemistry 55 (2016) 6996–7004.
[57] M. Sugiura, T. Tibiletti, I. Takachi, Y. Hara, S. Kanawaku, J. Sellés, A. Boussac, Probing the role of valine 185 of the D1 protein in the photosystem II oxygen evolution, Biochim. Biophys. Acta 1859 (2018) 1259–1273.
[58] H. Sakamoto, T. Shimizu, R. Nagao, T. Noguchi, Monitoring the reaction process during the $S_2 \rightarrow S_3$ transition in photosynthetic water oxidation using time-resolved infrared spectroscopy, J. Am. Chem. Soc. 139 (2017) 2022–2029.
[59] S. Styring, A.W. Rutherford, Deactivation kinetics and temperature-dependence of the S-state transitions in the oxygen-evolving system of photosystem-II measured by electron paramagnetic resonance spectroscopy, Biochim. Biophys. Acta 933 (1988) 378–387.
[60] H. Isobe, M. Shoji, S. Yamanaka, Y. Umena, K. Kawakami, N. Kamiya, J.-R. Shen, K. Yamaguchi, Theoretical illumination of water-inserted structures of the $CaMn_4O_5$ cluster in the S_2 and S_3 states of oxygen-evolving complex of photosystem II: full geometry optimizations by B3LYP hybrid density functional, Dalton Trans. 41 (2012) 13727–13740.
[61] H. Isobe, M. Shoji, J.-R. Shen, K. Yamaguchi, Chemical equilibrium models for the S_3 state of the oxygen-evolving complex of photosystem II, Inorg. Chem. 55 (2016) 502–511.
[62] M. Sugiura, Y. Ozaki, M. Nakamura, N. Cox, F. Rappaport, A. Boussac, The D1-173 amino acid is a structural determinant of the critical interaction between D1-Tyr161 (TyrZ) and D1-His190 in photosystem II, Biochim. Biophys. Acta 1837 (2014) 1922–1931.
[63] S. Styring, A.W. Rutherford, In the oxygen evolving complex of photosystem II the S0 state is oxidized to the S1 state by D+ (signal II slow), Biochemistry 26 (1987) 2401–2405.
[64] J.-L. Zimmermann, A.W. Rutherford, Photoreductant-induced oxidation of Fe^{2+} in the electron-acceptor complex of photosystem II, Biochim. Biophys. Acta 851 (1986) 416–423.
[65] A. Boussac, F. Rappaport, K. Brettel, M. Sugiura, Charge recombination in $S_nTyr_Z \cdot Q_A^- \cdot$ radical pairs in D1 protein variants of photosystem II: long range electron transfer in the Marcus inverted region, J. Phys. Chem. B 117 (2013) 3308–3314.
[66] P.E.M. Siegbahn, Computational investigations of S3 structures related to a recent X-ray free electron laser study, Chem. Phys. Lett. 690 (2017) 172–176.
[67] A. Boussac, Inhomogeneity of the EPR multiline signal from the S_2-state of the photosystem II oxygen evolving enzyme, J. Biol. Inorg. Chem. 2 (1997) 580–585.